Stochastic characterization and reconstruction of material microstructures for establishment of process-structure-property linkage using the deep generative model

Satoshi Noguchi and Junya Inoue

Phys. Rev. E **104**, 025302 — Published 9 August 2021

DOI: 10.1103/PhysRevE.104.025302

Stochastic characterization and reconstruction of material microstructures for establishment of process–structure–property linkage using the deep generative model

Satoshi Noguchi[1] and Junya Inoue[2, 3, 4, *]

[1] *Department of Advanced Interdisciplinary Studies, The University of Tokyo, 4-6-1 Komaba, Meguro, Tokyo 153-8904, Japan*
[2] *Institute for Industrial Science, The University of Tokyo, 5-1-5 Kashiwanoha, Kashiwa, Chiba 277-0082, Japan*
[3] *Department of Materials Engineering, The University of Tokyo, 7-3-1 Hongo, Bunkyo, Tokyo 113-8655, Japan*
[4] *Research Center for Advanced Science and Technology, The University of Tokyo, 4-6-1 Komaba, Meguro, Tokyo 153-8904, Japan*

(Dated: July 14, 2021)

In material design, microstructure characterization and reconstruction are indispensable for understanding the role of a structure in a process–structure–property relation. The significant contribution of this paper is to introduce a novel methodology for the characterization and generation of material microstructures using deep generative networks as the first step in the establishment of a process–structure–property linkage for forward/inverse material design. Our approach can be divided into two parts: (i) characterization of material microstructures by Vector Quantized Variational Auto-Encoder, and (ii) determination of the correlation between the extracted microstructure characterizations and the given conditions, such as processing parameters and/or material properties, by Pixel Convolutional Neural Network. As an example, we tested our framework in the generation of low-carbon-steel microstructures from the given material processing. The results were in satisfactory agreement with the experimental observation qualitatively and quantitatively, demonstrating the potential of applying the proposed method to forward/inverse material design. One of the advantages of the proposed methodology lies in the capability to capture the stochastic nature behind the microstructure generation. As a result, this methodology enables us to build a process–structure–property linkage while quantifying uncertainties, which not only makes a prediction more robust but also shows a way toward enhancing our understanding of the stochastic competitive phenomena behind the generation of material microstructures.

I. INTRODUCTION

The goal of materials design is to achieve inverse material design, the aim of which is to discover novel materials that have certain desired properties. The establishment of a process–structure–property linkage is indispensable for developing a general methodology for inverse material design and understanding the physical mechanisms behind materials microstructure generation [1–3]. For that purpose, a central problem is the analysis, characterization, and control of microstructures, since microstructures are highly sensitive to materials processing and critically affect material's properties. Thus, as a first step toward developing a methodology for inverse material design, the aim of this work is to consider a general methodology for the characterization and reconstruction of random heterogenous microstructures, which can lead to the establishment of a process–structure–property linkage.

Bostanabad et al. [4] listed major challenges in the building of a methodology for the characterization and reconstruction of microstructures: (i) how to efficiently and accurately quantify (characterize) the stochastic nature of high-dimensional data embedded in the material morphology and (ii) how to use this characterization to generate (reconstruct) virtual microstructure samples that are statistically equivalent, preserving as much of the inherent stochasticity as possible.

In recent years, machine-learning-based methods have received much attention in the field of computational material design [1, 4–12]. In particular, generative models are attracting considerable interest [13–19]. The task of generative models is to directly capture the stochastic generation process of the input data. Variational Auto-Encoder (VAE) [20] and Generative Adversarial Networks (GAN) [21] are two major algorithms of generative models. There have been a lot of works on modeling material microstructures and establishing process–structure–property relationship using VAE [22–24] and GAN [13, 15, 16, 25, 26].

VAE includes encoding and decoding networks. The encoder coverts an input datum into a low-dimensional vector known as a latent variable, and the decoder reproduce the original representation from the latent variable. On the other hand, GAN composes of generator and discriminator networks. Specifically, the generator tries to generate similar data to input from sampling noise, whereas the discriminator tries to distinguish data as synthetic or real. The goal of the training of GAN is that the generator is trained to produce data that cannot be identified as fake by the discriminator. In this way, GAN implicitly gives control over data generation by the discriminator, while VAE explicitly gives control over data generation via latent variables. The motivation of this work is developing a general methodology

for stochastic characterization and reconstruction of material microstructures as a basis of a data-driven framework to capture governing physical mechanisms behind material microstructure generation. For that purpose, because VAE-based models include an encoder network as a mapping from material microstructures into a latent space which is expected to disentangle physical correlations affecting material microstructure generation in latent space, VAE-based models are considered to be better choice than GAN-based models. Thus, in this work, we established our framework based on VQVAE, that is one of the VAE-based models.

We address the above two challenges for the characterization and reconstruction of material microstructures by applying two deep generative networks, namely, Vector Quantized Variational Auto-Encoder (VQVAE) [27] to challenge (i), that is, microstructure characterization, and Pixel Convolutional Neural Network (PixelCNN) [28, 29] to challenge (ii), that is, microstructure generation. The basic idea in this work is to consider the characterization and generation of material microstructures as a data-driven supervised learning using microstructure images with the corresponding process parameters and/or material properties as a training dataset. This work can be understood as an application of VQVAE and PixelCNN in the generation of material microstructures.

The following aspects are covered in this paper. (i) We propose the image-based general methodology for the characterization of materials microstructures by VQVAE. (ii) We propose to use PixelCNN to determine the relationship between the characterization of microstructures and any conditions users can select depending on their purpose, such as process parameters and/or material properties. (iii) We test the proposed framework on low-carbon-steel microstructures and show the potential of applying the proposed method to material design.

The main purpose of this paper is to introduce a novel methodology for the characterization and generation of material microstructures using deep generative networks as the first step in the establishment of a process–structure–property linkage for forward/inverse material design. The advantage of our approach is that the proposed method can capture the stochastic relationship between material microstructures and the given conditions by elucidating the microstructure characterizations and relating the characterizations to the given conditions, resulting in the establishment of a stochastic process–structure–property linkage. In other words, the proposed methodology allows us to build a stochastic mapping from the given conditions to the corresponding microstructures, which can be used to generate an ensemble of statistically equivalent microstructure samples. Also, because the introduced framework can be straightforwardly applied to relate the microstructure to the material properties, the proposed methodology can be the basis of the inverse material design in which the uncertainties resulting from the stochastic nature of microstructures are considered.

The rest of this paper is organized as follows. Section II explains the deep generative networks used in the proposed framework, and Section III gives results of an example of its application to low-carbon-steel microstructures. Then, we conclude the paper in Section IV.

II. METHODOLOGY

In this section, we introduce the deep learning algorithms used in our framework. Our fundamental idea is to consider the microstructure characterization and generation problem as data-driven supervised learning using microstructure images with the corresponding process parameters and/or material properties as the training dataset. The proposed methodology is composed of the two deep learning models, VQVAE [27] and PixelCNN [28, 29]. VQVAE is used for the extraction of the features of microstructure images to obtain their characterization, and PixelCNN is used to establish the relationship between the extracted characterizations and given conditions, such as process parameters and/or material properties. Because PixelCNN learns stochastic mapping from the given conditions to the feature space of microstructures, the introduced methodology enables us to stochastically predict the microstructures corresponding to the given conditions.

Fig. 1 shows a schematic of the procedure of our framework, which has three steps for the generation of new microstructures: (Training 1) characterization of microstructures by extracting features using VQVAE, (Training 2) correlation of the extracted features to the given conditions using PixelCNN, and (Prediction) generation of microstructures corresponding to the given condition using trained networks.

A. Vector Quantized Variational AutoEncoder (VQVAE)

First, we describe VQVAE used for characterizing the material microstructures. The task of VQVAE is to learn the stochastic generation process of the input data through latent variables. The input data are microstructure images here. Since VQVAE is related to Variational AutoEncoder (VAE) [20] and VQVAE shares basic ideas with VAE, we start with an explanation of the fundamental idea of VAE to describe the architecture of VQVAE.

VAE includes probabilistic encoder $Q(z|x)$ and probabilistic decoder $P(x|z)$ networks, which are modeled by convolutional neural networks; see Fig. 2. $Q(z|x)$ is defined as an approximation of the intractable true posterior $P(z|x)$. The encoder maps the input image to a vector following a probability distribution

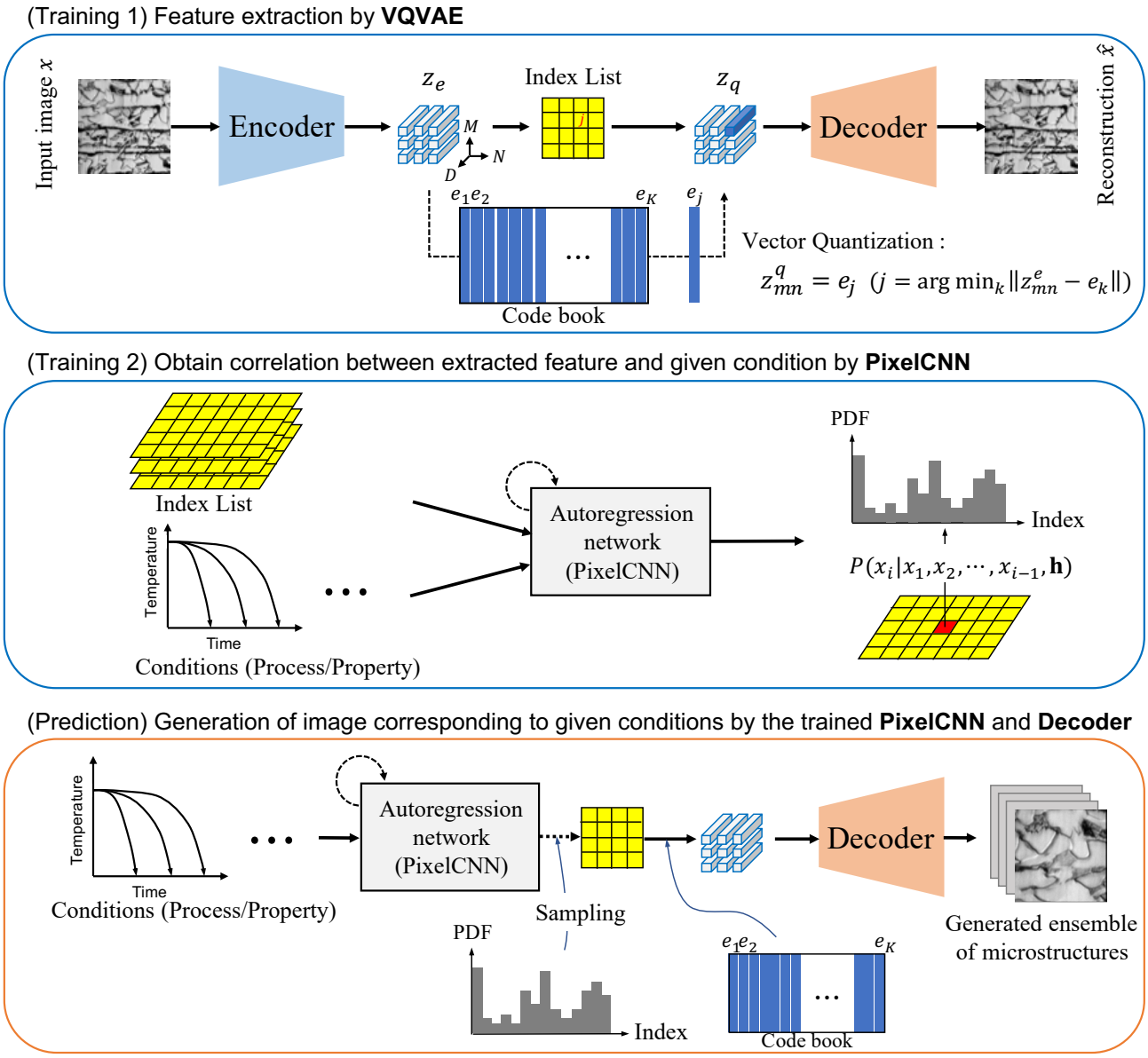

FIG. 1. Schematic of the procedure of the proposed framework. (Training 1) Characterization of microstructures by VQVAE [27]. As a result of VQVAE, we can extract index lists corresponding to input images, which are the input of PixelCNN in this framework. (Training 2) Determination of the correlation between extracted features and given conditions, such as process parameters and/or material properties, by PixelCNN [28, 29]. In its application to low-carbon-steel microstructures, the natural logarithm of the cooling rate was given to PixelCNN as an example of conditions $\mathbf{h}$. (Prediction) Microstructure generation using the trained networks. First, by using the trained PixelCNN, the index list is sampled from the probability distribution conditioned by the given parameter. Then, each index is replaced by the discrete latent vector in the codebook. Finally, the decoder can generate the corresponding microstructure from the set of latent vectors.

on a lower-dimensional space known as the latent space. The distribution is often Gaussian because of its useful numerical and theoretical properties. Specifically, the encoder has a fully connected layer as the final layer; thus, the encoder outputs a mean vector μ and a vector of the diagonal elements of covariance matrix σ that describe the Gaussian distribution, where the covariance matrix of the Gaussian distribution is usually assumed as the diagonal matrix. The decoder maps a latent vector sampled from the assumed distribution back to the original image, as shown in Fig. 2. In practice, the noisy vector is obtained by transforming the sampled Gaussian noise from the standard normal distribution $n \sim N(\mathbf{0}, \mathbf{I})$ using the mean and the covariance matrix $z = \mu + \sigma n$, where z is considered to be the sampled latent vector from the assumed Gaussian that is the input of

the decoder. Therefore, VAE must regenerate the input datum from the noisy vector. As a result, VAE can obtain the representation of the input datum not as a fixed point but as a probability distribution on the latent space. In the act of compressing and decompressing information, VAE is expected to extract some essential continuous features from the input images.
In VAE, the following error function is optimized (minimized) [20]. The error function is written as the sum of the reconstruction error and the Kullback–Leibler divergence error:

$$\mathcal{L}_{VAE} = ||x - \hat{x}||_2 + KL\left[Q(z|x)||P(z)\right]. \quad (1)$$

The first term is the mean squared error between the input data x and the regenerated data $\hat{x}$, and the second term can be written as

$$KL\left[Q(z|x)||P(z)\right] = \int Q(z|x)\log\frac{Q(z|x)}{P(z)}dz, \quad (2)$$

where $P(z)$ is assumed as a standard normal distribution as usual. This term acts like the regularization term; in other words, this term prohibits $Q(z|x)$ from being too complex distribution in the sense of being too different from the standard normal distribution.

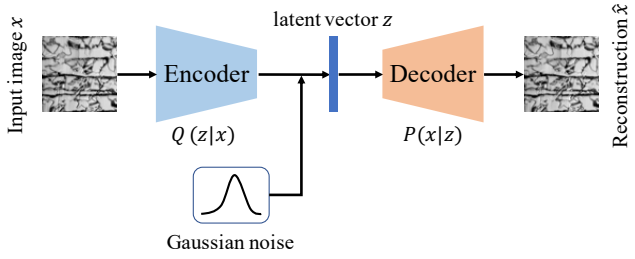

FIG. 2. Schematic of architecture of VAE.

VQVAE has been developed on the basis of the above VAE. The schematic of the architecture of VQVAE is shown in Fig. 1 (Training 1). VQVAE is also composed of a convolutional encoder and a convolutional decoder. However, while VAE has the continuous latent vectors that are usually assumed to follow Gaussian distribution, VQVAE has discrete latent vectors. VQVAE does not explicitly assume the distribution that the latent vectors follow; instead, VQVAE applies an additional vector quantization (VQ) procedure. In VQVAE, K discrete latent D-dimensional vectors are randomly sampled from the D-dimensional latent space. The set of K D-dimensional vectors is called *codebook* $e \in \mathbb{R}^{D\times K}$. These D-dimensional vectors are also optimized in the training. The latent vector z in VAE is replaced by two variables such as $z^e \in \mathbb{R}^{M\times N\times D}$ and $z^q \in \mathbb{R}^{M\times N\times D}$. z^e is the output of the convolutional encoder and is understood to be a set of $M \times N$ D-dimensional vectors in VQVAE, and z^q is the set of the nearest vectors in the codebook to the D-dimensional vectors included in z^e, as given by

$$z^q_{mn}(x) = e_j, \quad \text{where} \quad j = \text{argmin}_k||z^e_{mn}(x) - e_k||_2, \quad (3)$$

where e_k is a D-dimensional discrete latent vector included in the codebook. Unlike VAE, the output of the encoder is not directly used for the input of the decoder. Instead, the nearest D-dimensional vector in the codebook, e_j, according to Eq. (3) is used as the input of the decoder. The decoder regenerates the input image from a set of replaced discrete vectors z^q. This replacement procedure based on Eq. (3) in VQVAE is called the vector quantization procedure. Unlike in VAE, since the latent vectors of VQVAE are not forced to follow the unimodal Gaussian distribution, the latent vectors are expected to be more flexible. As a result, VQVAE can capture more sophisticated features than the usual VAE, leading to clearer and sharper reconstructed images.

The error function of VQVAE is composed of three error terms, reconstruction error, codebook error, and commitment error [27], as the first, second and third term in Eq. (4), respectively,

$$\mathcal{L}_{VQVAE} = ||x - \hat{x}||_2 + ||\phi_{sg}(z^e) - z^q||_2 + \beta||z^e - \phi_{sg}(z^q)||_2, \quad (4)$$

where ϕ_{sg} is the stopgradient operator and β is the weight for adjusting the influence of the commitment error. The reconstruction error is the same one as in the usual VAE. The codebook error is used for making chosen vectors included in codebook z^q approach the corresponding D-dimensional vectors in the output of encoder z^e, while the commitment error is applied for making vectors included in z^e close to the selected vectors in codebook z^q in D-dimensional space with respect to L^2-distance. ϕ_{sg} is introduced so that z^e and z^q can approach each other alternately. Note that the result is not sensitive to the value of β [27].

B. PixelCNN

Next, we describe PixelCNN, which is used for obtaining the relationship between the features extracted by VQVAE and the given conditions, such as process parameters and/or material properties. The schematic of the architecture is shown in Fig. 1 (Training 2). PixelCNN is an autoregressive model for building the joint distribution of pixels over an image $\mathbf{x}$ as the following product of conditional distributions [28, 29],

$$P(\mathbf{x}|\mathbf{h}) = \prod_{i=1}^{n^2} P(x_i|x_1, \cdots, x_{i-1}, \mathbf{h}), \quad (5)$$

where $\mathbf{x}$ represents the input image, x_i is a single pixel in the image, and $\mathbf{h}$ is the given condition. The conditional distribution written as Eq. (5) is modeled by a CNN that is connected to a softmax layer to estimate the

probability of n_c classes, depending on the problem. For example, in the case of estimating the probability of pixel values in an 8-bit single-channel image, $n_c = 256$. The ordering of the pixel dependences is left to right and top to bottom. In other words, every pixel is dependent on all pixels above and to the left of it; see Fig. 3. The network of PixelCNN is modeled to realize this dependence of pixels [28, 29]. Note that **h** does not depend on the location of the pixel in the image. This is equivalent to adding a condition-dependent bias at every layer of the network.

VQVAE can extract the index list corresponding to the input images, which is an $M \times N$-dimensional matrix composed of the indexes of the chosen vectors according to Eq. (3); see Fig. 1 (Training 1 and 2). Using the trained encoder of VQVAE, we can obtain index lists for all input images. For any index list, since it records only the indexes of the discrete latent vectors in the codebook, we can treat it as a single-channel image. Each *pixel* in the index list has K possible values, depending on the size of the codebook: $n_c = K$. In other words, PixelCNN can be used to model the possibility of K discrete values for each pixel based on the dependence of pixels shown in Fig. 3.

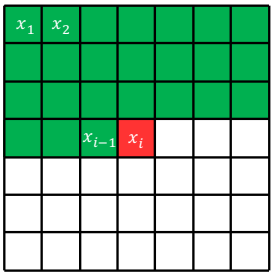

FIG. 3. Schematic of pixel dependences assumed in PixelCNN. The central red pixel x_i is dependent on the green pixels $x_1, x_2, \cdots, x_{i-1}$.

Modeling the probability distribution of the index lists by PixelCNN resembles the process for a low-resolution image. The inputs of PixelCNN are the index lists and the conditions that users can select. Then, the network is trained using the cross-entropy loss function for the expectation of the inference of the network to be identical to the true index list. After training, the network can capture the pattern of microstructure images in the latent space as a conditional distribution of index lists based on the preceding index order.

C. Microstructure generation

Using the trained networks, microstructures can be generated corresponding to the given conditions such as process parameters and/or material properties [28]. The schematic procedure of macrostructure generation is shown in Fig. 1 (prediction). First, the desired conditions are given to the trained PixelCNN to obtain the probability distribution of index lists. Each index is sampled on the basis of the obtained distribution in accordance with the preceding order. Since PixelCNN is an autoregressive model, we must generate the index list pixel by pixel. In practice, by inputting the zero matrix and the desired conditions to the PixelCNN, we obtain the first pixel's distribution. After sampling the value of the first pixel from the distribution, we update the input matrix by adding the first pixel value, and repeat this process until all pixel values are generated. Then, from the sampled index list, we can build a set of latent vectors that will be the input of the decoder, using the trained codebook. Finally, from the obtained latent vectors, the microstructure image is generated by the trained decoder. As a result, we can obtain the stochastic mapping from the given conditions to the corresponding microstructure images.

III. RESULTS OF APPLICATION TO STEEL MICROSTRUCTURES

A. Training dataset of steel microstructures

In this section, to illustrate the potential of the proposed methodology for microstructure characterization and generation, the proposed methodology is applied to cold-rolled (CR) low-carbon-steels under different process conditions and the obtained results are shown. The CR steel samples were austenitized at 1000 °C and cooled at 1.0, 3.0, 10.0, or 30.0 °C/s to room temperature. Then, they were polished and etched using picral solution. The details about preparation of steel microstructure images can be found in [7]. Note that in this reference, the microstructure corresponding to the cooling rates 1.0, 3.0, 10.0, and 30.0 °C/s are referred to as A10-01, A10-03, A10-10, and A10-30, respectively. Fig. 4 shows examples of the prepared steel microstructure images.

To create a training dataset, square patches (128 × 128 pixel) are cropped from the original microstructure images (1024 × 768 pixel), and the cropped patches are converted to grayscale images; see Fig. 5. We cropped 165 square images overlapping with each other for each original microstructure image. In addition, we added the square images flipped horizontally to the training dataset, which are also 165 square images for each original microstructure image. As a result, since we can crop 330 square images from one original microstructure image, the training dataset includes 52,800 grayscale images cropped from 160 original microstructure images of 40 observed microstructures for each of the four cooling rates 1.0, 3.0, 10.0, and 30.0 °C/s.

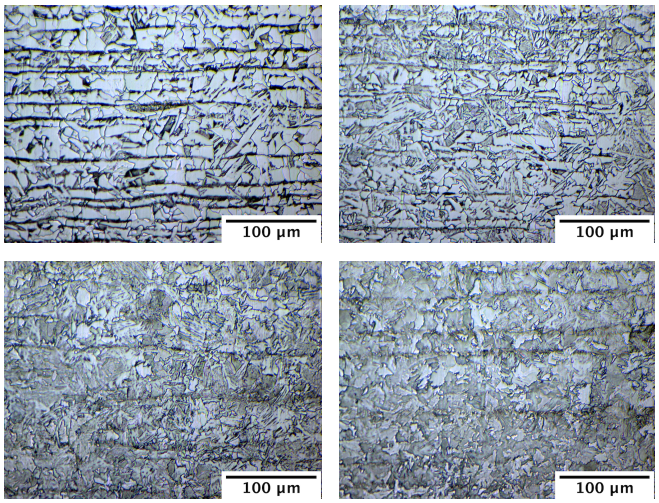

FIG. 4. Examples of original microstructure images. The size of the images is 1024 × 768 pixel, and 1 pixel is 0.34 μm × 0.34 μm in these microstructure images. The upper left, upper right, lower left, and lower right images show the steel microstructures cooled at 1.0, 3.0, 10.0, and 30.0 °C/s, respectively. The total number of prepared images is 160 and comprise 40 microstructure images for each of the four cooling rates 1.0, 3.0, 10.0, and 30.0 °C/s.

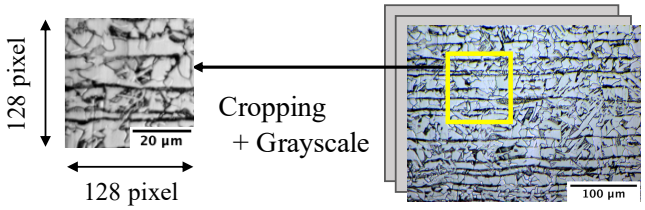

FIG. 5. Schematic of procedure of creating the training dataset from the original microstructure images. 128 × 128 pixel patches are cropped and then converted to grayscale images.

B. Results of application to the steel microstructures

We trained each network by the procedure presented in Fig. 1 (Training 1) and (Training 2). First, using the prepared training microstructure image dataset, VQVAE was trained as shown in Fig. 1 (Training 1). In this application, we set M, N, and D in the architectures of VQVAE and PixelCNN as 16, 16, and 128, respectively. Also, the number of prepared latent vectors in codebook K is set as 512. Fig. 6 presents the microstructure images reconstructed after training with the corresponding training microstructure images. This result illustrates that VQVAE can reproduce sharp and clear microstructure images.

Then, PixelCNN was trained using index lists obtained by the trained VQVAE and the corresponding cooling rates as shown in Fig. 1 (Training 2). In this application, the natural logarithm of the cooling rate was adopted as a condition **h** in PixelCNN. As a result of training, we can obtain stochastic mapping from the cooling rate to the corresponding microstructures as shown in Fig. 1 (Prediction).

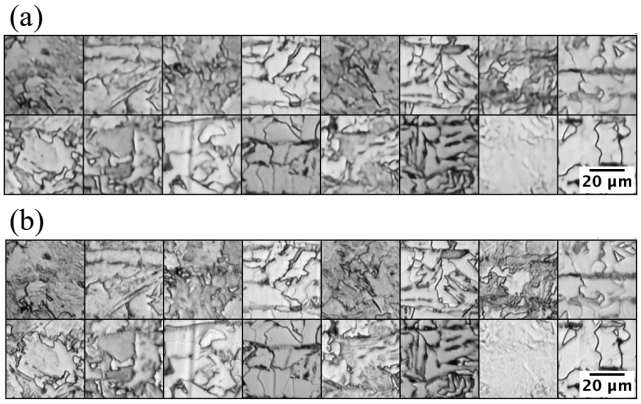

FIG. 6. Image reconstruction by VQVAE. (a) Microstructure images reconstructed by VQVAE. (b) Corresponding original microstructure images. This result shows that VQVAE can reproduce sharp and clear microstructure images.

Using the mapping obtained from the results of the trained networks, we can generate new microstructures corresponding to any cooling rate. Fig. 7 presents the generated microstructures corresponding to the given cooling rates by the proposed methodology along with the sampled training images in the dataset for each cooling rate. These results indicate that the proposed method can produce qualitatively realistic microstructure images for each cooling rate in the sense that the generated microstructures have similar features to those observed in training microstructure images in terms of the basic topology of microstructures and a similar trend relative to the change in the cooling rate. It should be emphasized that the introduced method can generate new microstructures in the sense that the generated microstructure images are not exactly the same as the images in the training microstructure dataset. In addition, the significance of our approach is that this method can create an ensemble of microstructures illustrating the distribution of material microstructures conditioned by the given parameters. In other words, the generated images in Fig. 7 can be understood to be the results of sampling from the distribution of microstructures modeled by the proposed method; this can lead to the establishment of the process–structure linkage with uncertainty taken into consideration.

In addition, the proposed method can generate the microstructures corresponding to the interpolated cooling rates but were not included in the training dataset. Fig. 8 shows the generated microstructures corresponding to the interpolated cooling rates 2.0, 6.5, and 20.0 °C/s. The trend of microstructures relative to the change in the cooling rate seems to be captured with respect to the basic morphology of

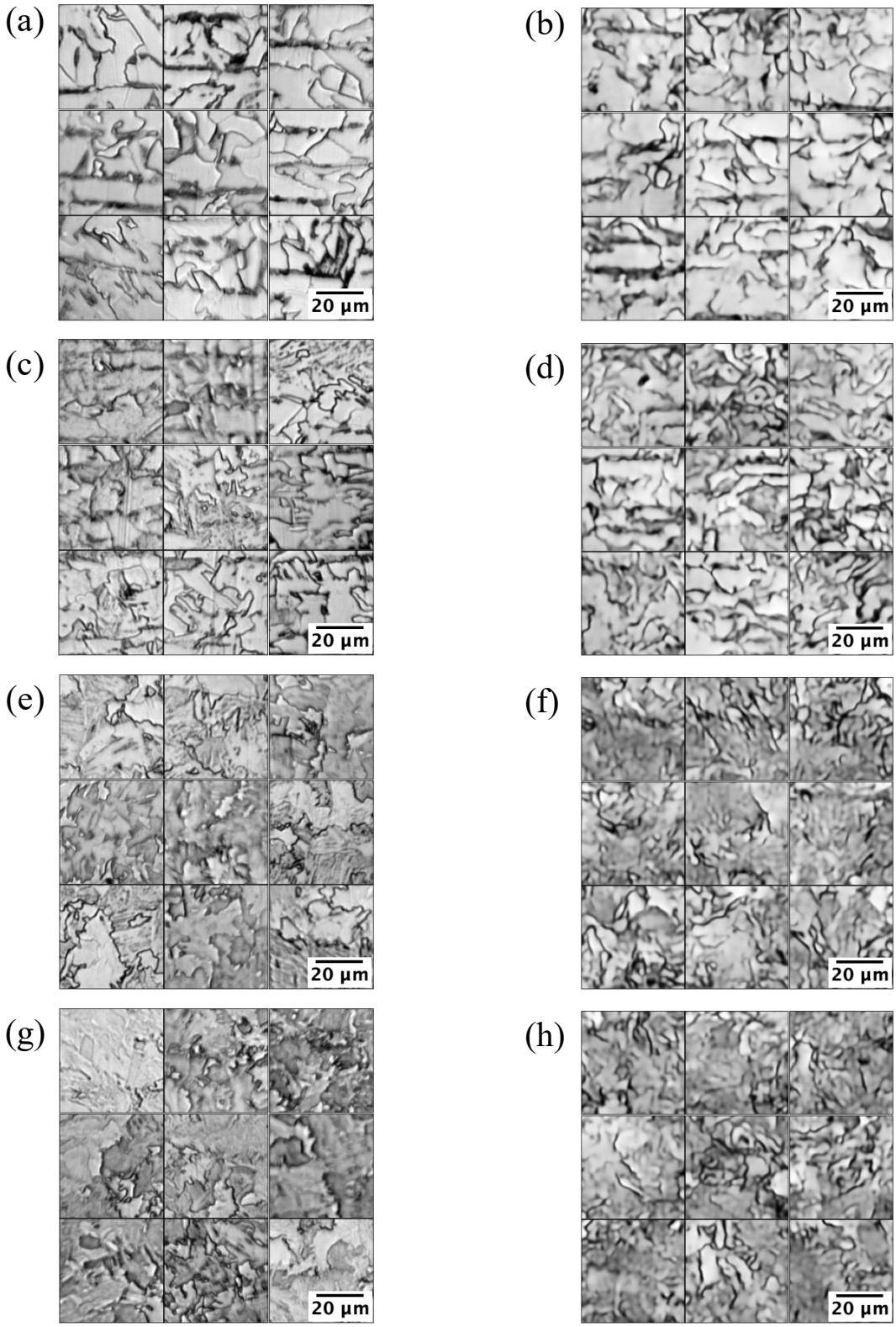

FIG. 7. Original microstructure images and generated microstructure images corresponding to the given cooling rates. (a), (c), (e), and (g) are original microstructures for each of the four cooling rates 1.0, 3.0, 10.0, and 30.0 °C/s, respectively. (b), (d), (f), and (h) are generated microstructures for each of the four cooling rates 1.0, 3.0, 10.0, and 30.0 °C/s, respectively. Each set shows nine microstructure images.

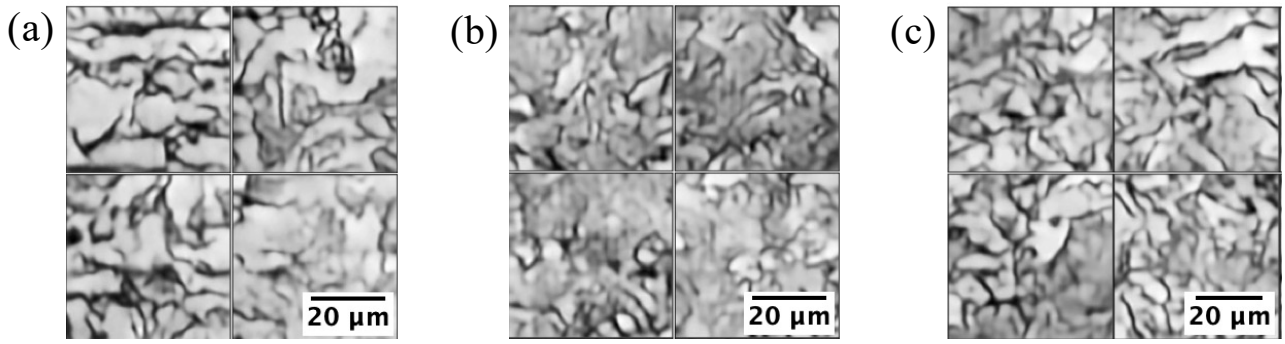

FIG. 8. Microstructure interpolation. (a), (b), and (c) are generated microstructure images corresponding to the cooling rates 2.0, 6.5, and 20.0 ° C/s, respectively, which were not included in the original dataset. Regarding microstructure morphology, trained VQVAE seems to capture the trend relative to the change in cooling rate. Each set shows four microstructure images.

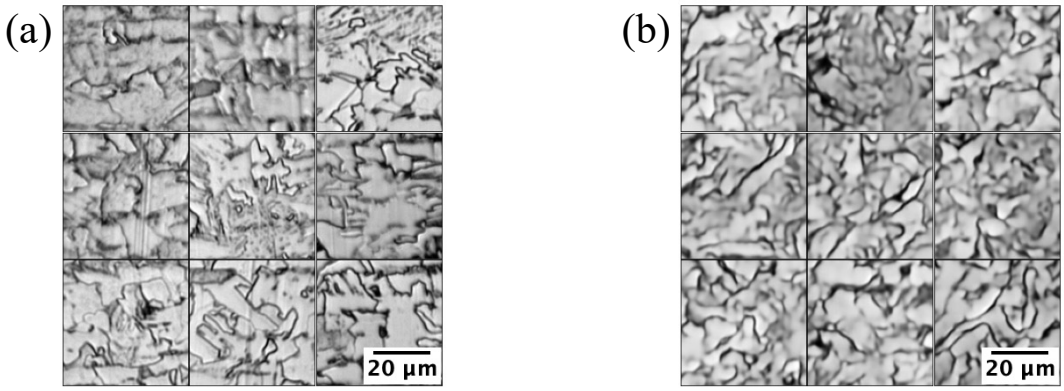

FIG. 9. Original microstructures observed in the experiment and microstructures predicted by our approach. (a) and (b) are respectively original and predicted microstructures for cooling rate 3.0 °C/s. We can see that the predicted microstructures have similar topology to the original microstructure images. This result validates the capability of the proposed method to predict the microstructures corresponding to interpolated conditions. Each set shows nine microstructure images.

microstructures. Although more careful discussion is needed, this result shows the significant potential of the presented methodology.

To validate the capability of the proposed method to generate new microstructures corresponding to the interpolated cooling rates, we trained the networks using the training dataset without the microstructure images corresponding to the cooling rate 3.0 ° C/s. After training, we compare the microstructure images corresponding to the cooling rate 3.0 ° C/s in the original dataset with the microstructures predicted by the networks trained with the limited dataset. Fig. 9 presents the results of validation. In terms of the basic morphology of microstructures, such as the composition of black and white microstructures and the grain sizes, the prediction is in acceptable agreement with the microstructures observed in experiments. This result validates the capability of the proposed method to predict the microstructures corresponding to the interpolated conditions.

To validate the generated microstructures quantitatively, we consider two descriptors of microstructure morphology: the volume fraction and the average grain size. From the physical viewpoint, since the picral solution lightly colors ferrite in the microstructure, the proportion of white region in the microstructure is considered to correspond to the volume fraction of ferrite. Thus, in the rest of this paper, the ratio of the white region to the total area of a unit patch of microstructure (128×128 pixel) is used synonymously with the ferrite volume fraction. We calculated the ratio of the white region to the total area in the cropped patches of microstructures. First, we binarized the microstructure patches by Otsu's method [30]. Then, the ratio of white pixels in a patch (128×128 pixel) was calculated for 1000 training and 1000 generated images for each of the four cooling rates 1.0, 3.0, 10.0, and 30.0 ° C/s. Also, the mean and the variance were calculated for each set of images. Fig. 10 shows the box plot of the calculated ferrite volume fraction for the training images and the generated images corresponding to each cooling rate. Table I presents the results of the calculated means and variances.

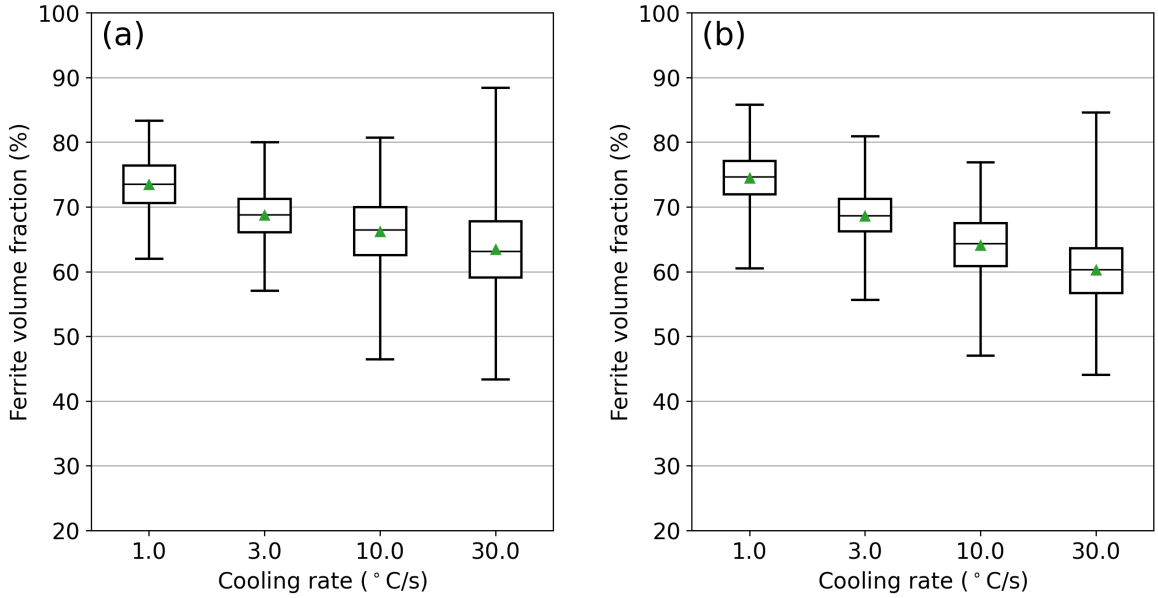

FIG. 10. Box plots of the ferrite volume fractions in (a) the microstructure patches cropped from the original images, and (b) the microstructure patches generated by the introduced methodology. The black lines and green triangles in the boxes denotes median and mean values of sets of images for each cooling rate, respectively. Larger variance corresponds to higher spatial variation of microstructures.

TABLE I. Calculated means and variances of the ferrite volume fractions of 1000 training and 1000 generated images for each of the four cooling rates 1.0, 3.0, 10.0, and 30.0 °C/s.

	Cooling rate (°C/s)	1.0	3.0	10.0	30.0
Mean (%)	Training images	73.4	68.8	66.2	63.4
	Generated images	74.4	68.6	64.1	60.3
Variance (%^{2})	Training images	15.8	13.9	29.3	50.3
	Generated images	14.9	14.3	25.8	30.0

In terms of mean values, the ferrite volume fractions of the generated images for all cooling rates are in satisfactory agreement with those of the training images. Also, the volume fraction of ferrite in the generated images in Fig. 10 clearly shows the similar trend of variances to the original observed microstructures; as the cooling rate increases, the variance of the volume fraction of ferrite also increases. Since the images used for the calculation of the volume fraction were local microstructure images cropped from the larger original microstructure images of 1024 × 768 pixels, the higher variance means a larger spatial variation of microstructures. Therefore, these results indicate that the proposed method can reveal the effect of the cooling rate on the behavior of microstructures including the stochastic spatial variation. In this sense, the proposed method can be considered to capture the stochastic relationship between the given process parameters and the corresponding microstructures.

Next, we consider the average grain size in a micrograph. In this paper, as a variable corresponding to the average grain size, the mean free path d_f defined in [31] is used. The mean free path is also calculated for the binarized microstructure images. d_f is defined as

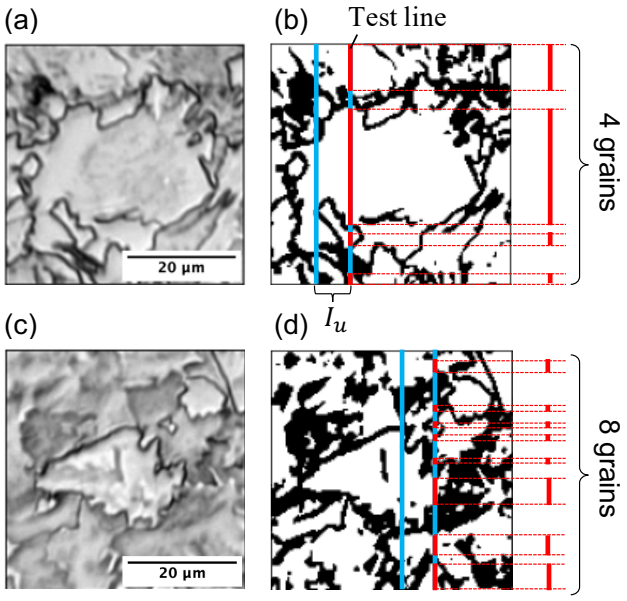

FIG. 11. Original microstructure patches ((a) and (c)) and schematic figures for the calculation of the mean free path ((b) and (d)). The example test line passes through four white grains in (b) and eight white grains in (d). The mean free path corresponds to the average of the segments of the test lines shown as the red lines in these figures.

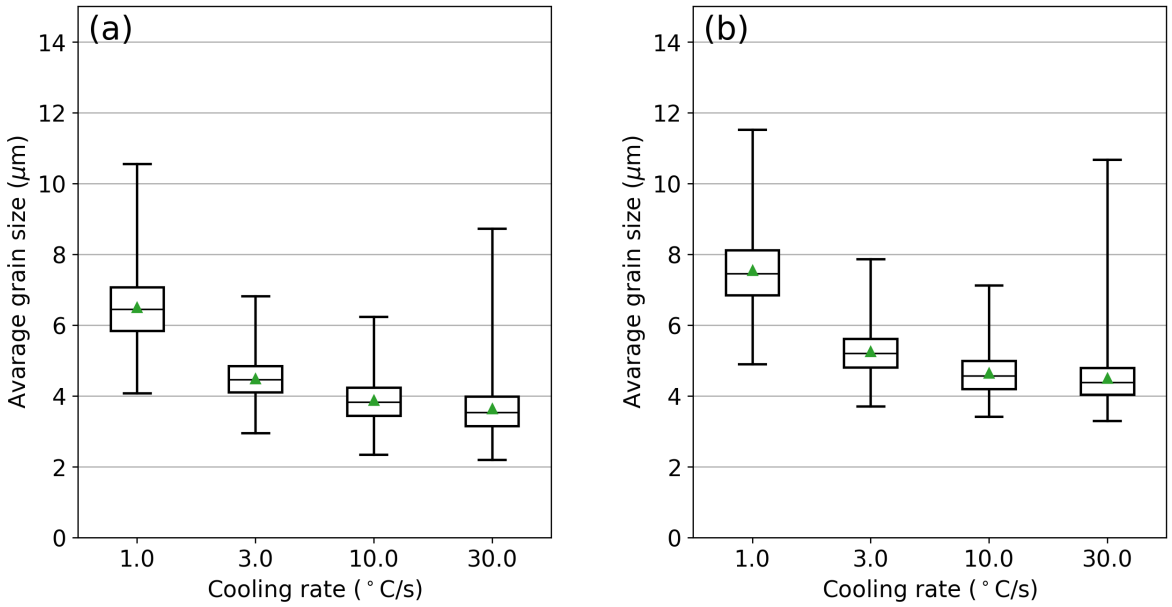

FIG. 12. Box plots of the average grain sizes (a) in each patch cropped from the original images, and (b) in each generated microstructure patch by the introduced methodology. The black lines and green triangles in the boxes denote median and mean values of sets of images for each cooling rate, respectively. The mean values are corresponding to the overall averages for each cooling rate. Note that 1 pixel is 0.34 μm $\times$ 0.34 μm in the microstructure images.

$d_f = V_f/(N_L \cdot I_u)$, where V_f is an area of the white region in a binarized microstructure images and N_L is the total number of white grains that test lines pass through in a microstructure image; see Fig. 11. The test lines are drawn in the unit interval I_u vertically or horizontally. The final mean free path for a micrograph is calculated by averaging the mean free paths calculated for the set of vertical test lines and the set of horizontal test lines. Physically, it represents the average linear distance in one grain without encountering an obstacle in a micrograph.

In the present study, two kinds of average grain size based on the mean free path are considered; one is the overall average which is derived by averaging mean free paths for all prepared square patches, while another the local average obtained by assuming that the mean linear intercept length in each cropped micrograph is representing the average grain size in the corresponding region of interest. Even though each cropped area is not large enough to give a statistically satisfactory number of intercepts, we use the measure to quantify the spatial variation of grain size in each microstructure. Consequently, Fig. 12 reveals the variation in the overall average grain size for each cooling rate as well as the spatial distribution of the local average.

Fig. 12 shows the box plots of the local average grain sizes and their mean values as the overall averages for each patch cropped from original microstructures and the generated images. The local average grain sizes are calculated for 1000 training and 1000 generated images for each of the four cooling rates 1.0, 3.0, 10.0, and 30.0 °C/s, where 1 pixel is 0.34 μm $\times$ 0.34 μm in the microstructure images. Also, Table II presents the means and variances of the sets of local average grain sizes for each cooling rate. The trend of the predicted overall and local average grain sizes are in good agreement with the trend of the overall and local grain sizes calculated using the original microstructure images. In this sense, this result indicates that our approach can also capture the trend of the average grain size of microstructures from the given parameters including the stochastic spatial variation. Finally, from the results of the ferrite volume fraction and the average grain size, we can quantitatively validate the capability to predict the microstructures corresponding to the given cooling rates in terms of the morphology of material microstructures.

TABLE II. Calculated means and variances of the average grain sizes of 1000 training and 1000 generated images for each of the four cooling rates 1.0, 3.0, 10.0, and 30.0 °C/s. Note that 1 pixel is 0.34 μm $\times$ 0.34 μm in the microstructure images.

	Cooling rate (°C/s)	1.0	3.0	10.0	30.0
Mean (μm)	Training images	6.50	4.49	3.88	3.64
	Generated images	7.54	5.26	4.65	4.50
Variance (μm^2)	Training images	0.857	0.346	0.361	0.528
	Generated images	1.03	0.398	0.365	0.543

As a supplement to Fig. 10 (b) and Fig. 12 (b), the ferrite volume fractions and the average grain sizes are also calculated for the interpolated cooling

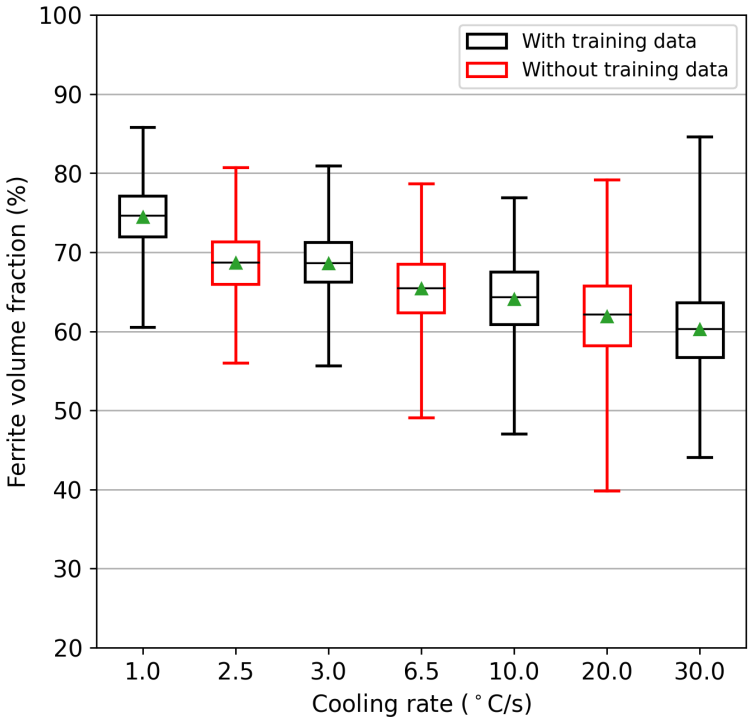

FIG. 13. Stochastic relationship between the cooling rate and the ferrite volume fraction in the microstructure patches predicted by the proposed methodology. The black lines and green triangles in the boxes denote median and mean values of sets of images for each cooling rate, respectively.

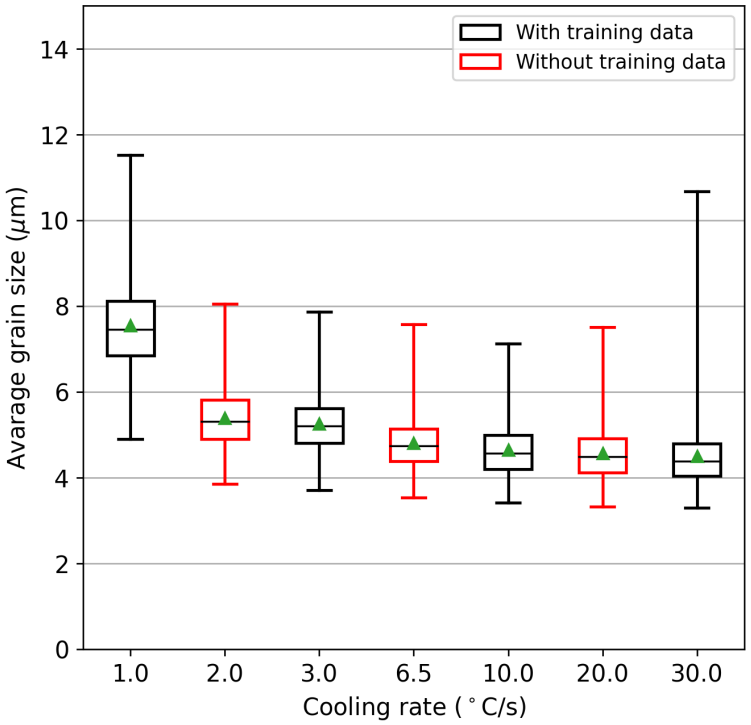

FIG. 14. Stochastic relationship between the cooling rates and the average grain sizes in the microstructure patches predicted by the proposed methodology. The black lines and green triangles in the boxes denote median and mean values of sets of images for each cooling rate, respectively. Note that 1 pixel is 0.34 μm $\times$ 0.34 μm in the microstructure images.

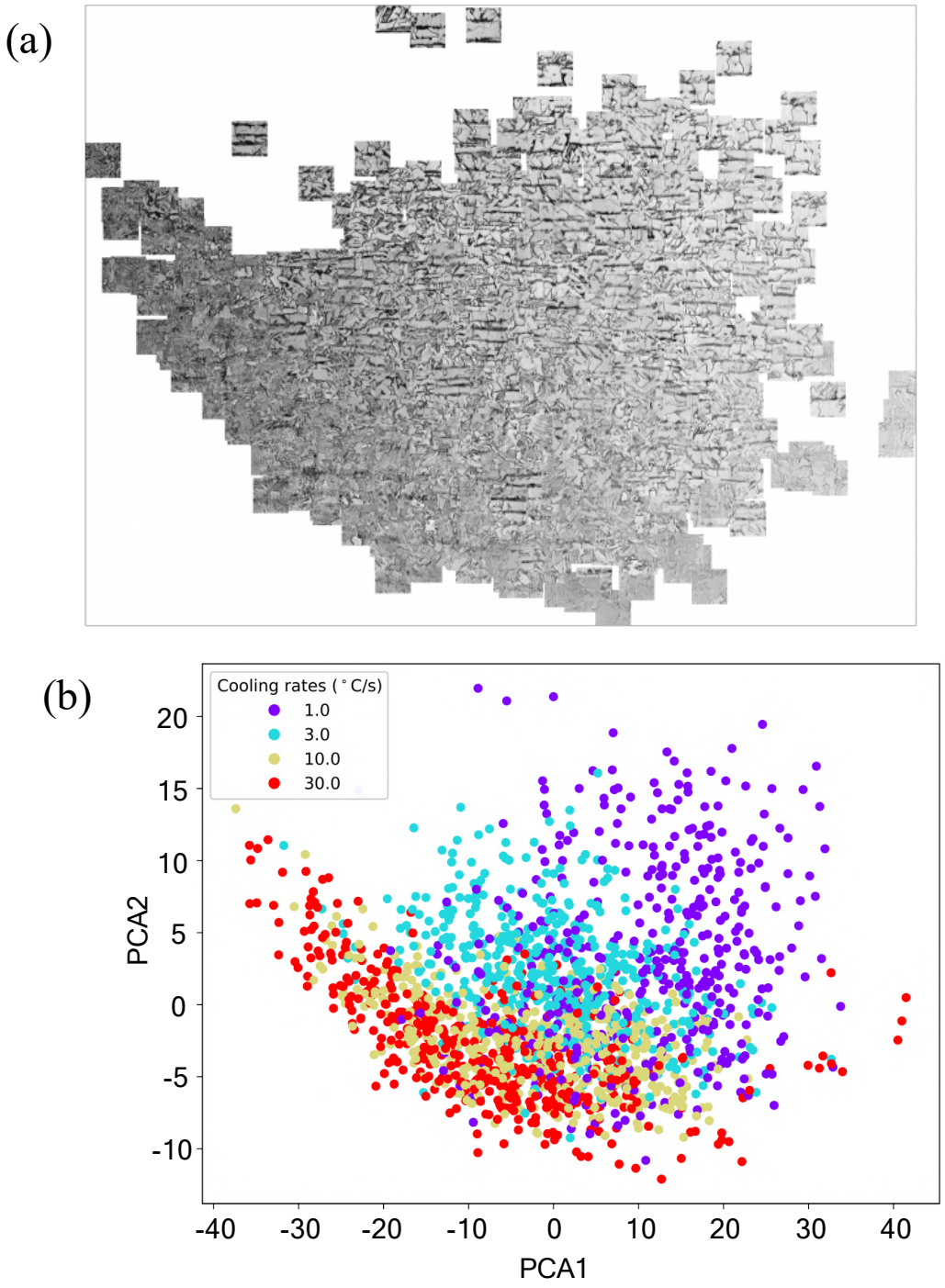

FIG. 15. Plots of microstructure images in the latent space with the corresponding cooling rates, visualized by PCA [32]. (a) Plot of images embedded in the latent space. (b) Plot of latent vectors colored for cooling rates.

rates not included in the training dataset, such as 2.0, 6.5, and 20.0 °C/s. The box plots of all results of ferrite volume fractions and average grain sizes are presented in Fig. 13 and Fig. 14. The trend of the ferrite volume fraction and the average grain size with respect to the cooling rate seem to be satisfactorily captured. Although more quantitative discussion is needed, these results might indicate the significant potential of the proposed methodology as a predictor.

The above results suggest that the introduced methodology can predict the basic morphology of microstructures, such as the composition of microstructure phases and the average grain size, from the given process parameters. In its application to steel

microstructures, the volume fraction of ferrite and the average grain size can be predicted, including the spatial variation. Moreover, the volume fraction and the average grain size are known as the dominant factors determining the strength of steels [7, 31, 33, 34]. Therefore, this result implies that we can predict the strength of the steel microstructures generated from the given processing parameters. This means that we can partially establish the process–structure–property relation, taking into consideration the uncertainty of the prediction due to the stochastic nature of microstructure generation, via the characterization of material microstructures by VQVAE and the determination of the stochastic relation between the characterization and the target parameters by PixelCNN.

Next, to better understand how the input microstructure patches are clustered and related in the feature space (latent space) extracted by VQVAE, we visualize the microstructures patches embedded in the latent space using principal component analysis (PCA) [32]. In practice, after the output tensors of the trained encoder in VQVAE corresponding to the input images are flattened into vectors, the vectors are compressed into two-dimensional vectors by PCA. Then, we map the microstructure patches in two-dimensional space in accordance with the compressed vectors. Fig. 15 (a) illustrates the result of the visualization of 2000 sampled patches randomly selected from the training dataset. This result shows that the patches seem to be mapped on the basis of the morphology of microstructures. We can see the continuous change of the microstructures in terms of the basic topology in the latent space. For example, the darker images are mapped in the left of Fig. 15 (a) and the lighter images are mapped in the right. Also, the grain sizes of microstructures are larger in the upper part of Fig. 15 (a). Fig. 15 (b) shows that the corresponding cooling rates are mapped in the same positions as the microstructures. Although the clusters corresponding to each cooling rate seem to be overlapped in the two-dimensional space, the microstructures for each cooling rate are clustered. Considering that the microstructure images are continuously distributed, the overlapped microstructures for different cooling rates are similar to each other in terms of the morphology of microstructures. Even though further investigation is needed to understand the physical background of this mapping of the microstructures, this result also demonstrates the potential of the proposed methodology.

From these results, this work shows the clear path to discuss material microstructure generation through the framework composed of VQVAE and PixelCNN. This framework gives the general data-driven methodology which could be applied for modeling and understanding a wide range of physical systems such as disordered condensed matters and amorphous/glassy materials. Future work will focus on the investigation about establishment of a methodology for making it possible to obtain physical knowledge based on the proposed framework. We provide the visualizations of the probability distribution of material microstructures in the latent space captured by PixelCNN in the appendix section, that could be a starting point for future investigation.

IV. CONCLUSION

As a first step in inverse material design, in this paper, we proposed a general methodology for the characterization and generation of material microstructures using two deep generative networks, Vector Quantized Variational Auto-Encoder (VQVAE) and PixelCNN. The fundamental idea of our approach is to consider the characterization and generation problems as data-driven supervised learning using the microstructure images as a training dataset. VQVAE was used for characterizing microstructures and PixelCNN was used for obtaining the correlation between the characterization and the given conditions such as processing parameters and/or material properties. Our work can be considered as an application of VQVAE and PixelCNN in the generation of material microstructures. To illustrate the potential of the introduced methodology, we applied the proposed method to the generation of steel microstructures from the given cooling rates as an example of material microstructure generation from selected process parameters and/or material properties.

As a result, the microstructures generated from given cooling rates by our methodology are in satisfactory agreement with the microstructures observed in experiments qualitatively in terms of the basic topology and quantitatively in terms of the ferrite volume fraction and the average grain size. Since the volume fraction and the average grain size are the dominant factors determining the strength of steels, this result implies that we can build the process–structure–property relation by the introduced methodology.

It should also be noted that the generated microstructure images are not the same as those in the training dataset. Therefore, the introduced method can generate new microstructures from the given cooling rates owing to the sophisticated characterization of microstructures by VQVAE. The significance of our methodology lies in the capability to directly model the distribution of microstructures conditioned by the given parameters such as the cooling rate. In other words, our method can capture the inherent stochastic nature that the training microstructures dataset may have and generate new microstructures while preserving the stochastic nature from the given conditions. This implies that our approach can capture the stochastic generation process of microstructures from the cooling rates; this can be a first step toward enhancing our understanding of the stochastic competitive phenomena behind microstructure generation.

The results of application to steel microstructures

also suggest that our method enables us to obtain the stochastic mapping from given processing parameters to material microstructures, which means that we can obtain the stochastic process–structure relationship by the proposed method. In the same way, the extracted features of microstructures can be related to material properties, which results in the stochastic mapping from the material properties to the corresponding microstructures. Thus, the introduced methodology can be straightforwardly applied to inverse material design by giving the target properties as conditions to PixelCNN. Therefore, our method allows us to stochastically predict the microstructures from particular desired properties, including the uncertainties. In conclusion, our approach can be a basis of establishing a stochastic process–structure–property linkage for inverse material design with uncertainty quantification.

DATA AVAILABILITY

The code is available at `https://github.com/inouejunyalab/for_public/tree/main/VQVAE_PixelCNN`. Also, original microstructure images are available from the corresponding author upon reasonable request.

ACKNOWLEDGMENTS

This work was supported by the Council for Science, Technology and Innovation, Cross-ministerial Strategic Innovation Promotion Program (SIP), "Structural Materials for Innovation" (funding agency: JST).

Appendix: Visualization of the distribution of material microstructures in the latent space

To demonstrate a potential of our framework to capture governing physical mechanisms behind material microstructure generation, we provide the probability distributions of material microstructures for each cooling rate in the latent space given by PixelCNN in the case of low-carbon-steel. As described in the main part of this paper, PixelCNN can provide a stochastic mapping from the given conditions such as processing parameters and/or material properties to the corresponding index lists. Since each index corresponds to geometrical feature which can be decoded to a certain microstructural image using the decoder of VQVAE, PixelCNN can be understood to provide a distribution of material microstructures conditioned by the given processing parameters and/or material properties in the latent space.

Fig. 16 visualizes vectors included in the trained codebook using primary component analysis (PCA) [32]. In practice, each 128-dimensional vector included in the codebook is mapped into two-dimensional vector by PCA. Fig. 16 is a plot of the compressed vectors in two-dimensional space. Their colors are determined based on the coordinate along the first primary component (horizontal direction). Thus, the similarity of colors corresponds to the spatial location of each vector in the latent space. Then, based on this coloring, sampled index lists are also colored. Fig. 17 shows the generated microstructures for each cooling rate and the corresponding colored index lists. Fig. 17 (b), (d), (f), and (h) can be regarded as the visualizations of the probability distributions of material microstructures for each cooling rate in the latent space. From the material viewpoint, these figures are visualizations of stochastic process–structure relation captured by PixelCNN. From these results, it is expected that PixelCNN can extract a part of governing physical mechanisms behind the generation of material microstructures affected by the change in cooling rate. Actually, as the cooling rate becomes higher, the number of pink or blue pixels increase in the index lists, which seem to be corresponding to the darker areas in the generated microstructure images.

To make our methodology more attractive for material design, understanding these index lists from the physical viewpoint need to be done, which will be provided in the future study.

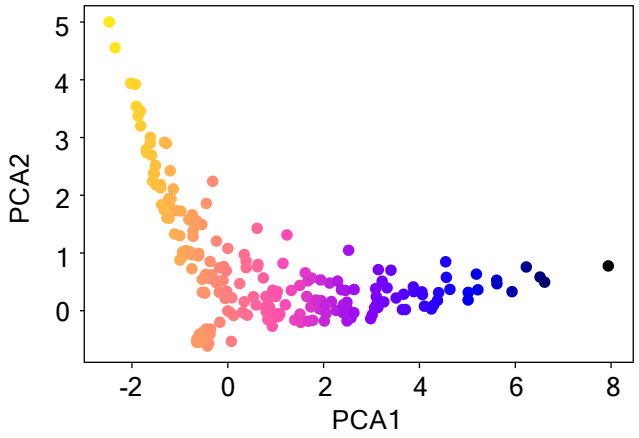

FIG. 16. A plot of the vectors included in the codebook colored based on the coordinate along the first main axis (horizontal direction) in PCA.

* Corresponding author
junya_inoue@metall.t.u-tokyo.ac.jp

[1] R. Bostanabad, Y. Zhang, X. Li, T. Kearney, L. C.

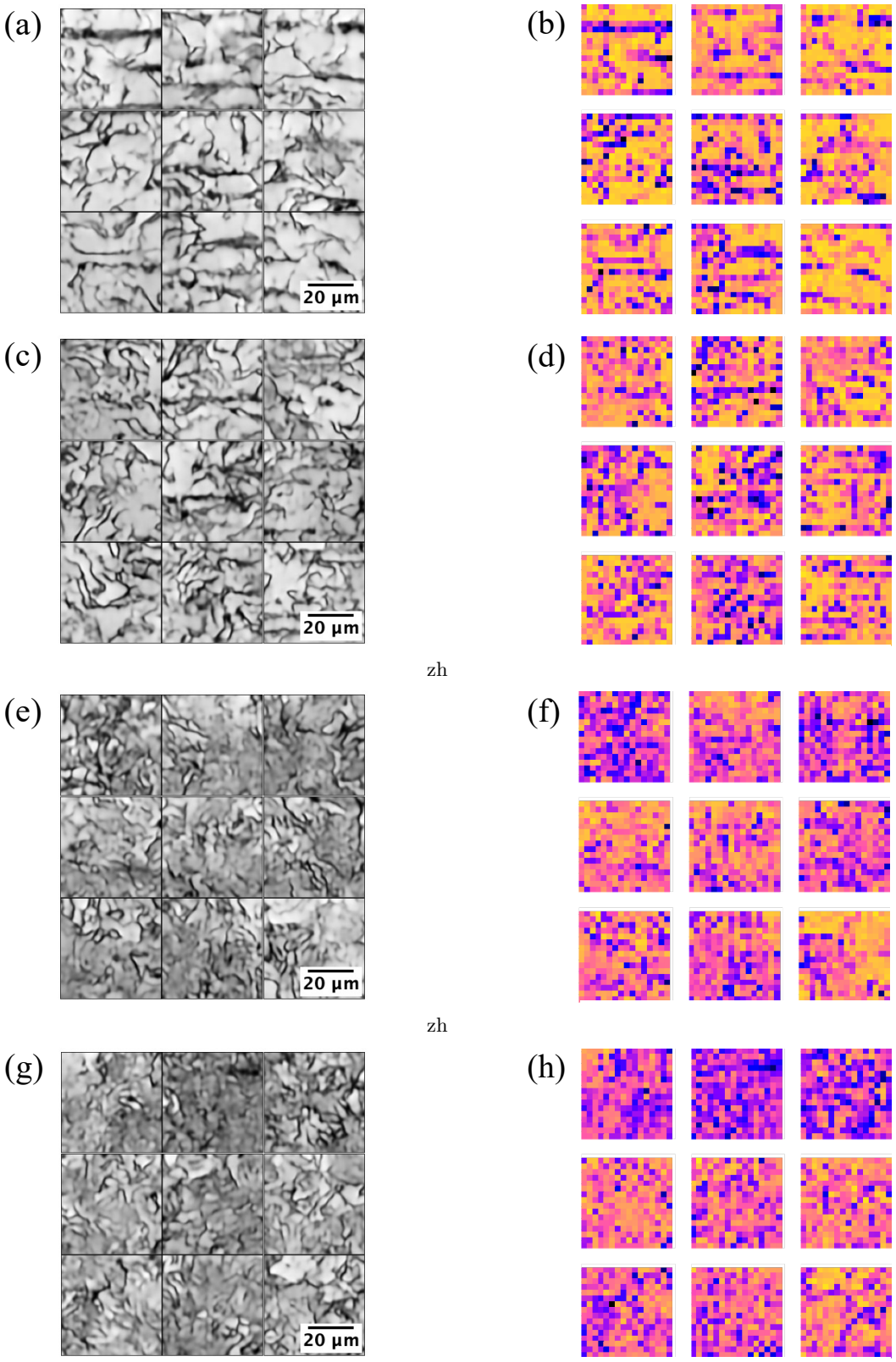

FIG. 17. Generated microstructure images and sampled index lists. (a), (c), (e), and (g) are generated microstructures for each of the four cooling rates 1.0, 3.0, 10.0, and 30.0 °C/s, respectively. (b), (d), (f), and (h) are sampled index lists for each of the four cooling rates 1.0, 3.0, 10.0, and 30.0 °C/s, respectively. We can see the correspondence between the generated microstructure images and sampled index lists. Each set shows nine microstructure images and index lists.

Brinson, D. W. Apley, W. K. Liu, and W. Chen, Computational microstructure characterization and reconstruction: Review of the state-of-the-art techniques, Prog. Mater. Sci. **95**, 1 (2018).

[2] A. Agrawal and A. Choudhary, Perspective: Materials informatics and big data: Realization of the fourth paradigm of science in materials science, APL Mater. **4**, 053208 (2016).

[3] G. B. Olson, Computational design of hierarchically structured materials, Science **277**, 1237 (1997).

[4] R. Bostanabad, A. T. Bui, W. Xie, D. W. Apley, and W. Chen, Stochastic microstructure characterization and reconstruction via supervised learning, Acta Mater. **103**, 89 (2016).

[5] R. Bostanabad, W. Chen, and D. Apley, Characterization and reconstruction of 3d stochastic microstructures via supervised learning, J. Microsc. **264**, 282 (2016).

[6] B. L. DeCost, T. Francis, and E. A. Holm, Exploring the microstructure manifold: image texture representations applied to ultrahigh carbon steel microstructures, Acta Mater. **133**, 30 (2017).

[7] Z.-L. Wang and Y. Adachi, Property prediction and properties-to-microstructure inverse analysis of steels by a machine-learning approach, Mater. Sci. Eng. A **744**, 661 (2019).

[8] Z. Yang, Y. C. Yabansu, R. Al-Bahrani, W. keng Liao, A. N. Choudhary, S. R. Kalidindi, and A. Agrawal, Deep learning approaches for mining structure-property linkages in high contrast composites from simulation datasets, Comput. Mater. Sci. **151**, 278 (2018).

[9] A. Cecen, H. Dai, Y. C. Yabansu, S. R. Kalidindi, and L. Song, Material structure-property linkages using three-dimensional convolutional neural networks, Acta Mater. **146**, 76 (2018).

[10] Z. Yang, Y. C. Yabansu, D. Jha, W. keng Liao, A. N. Choudhary, S. R. Kalidindi, and A. Agrawal, Establishing structure-property localization linkages for elastic deformation of three-dimensional high contrast composites using deep learning approaches, Acta Mater. **166**, 335 (2019).

[11] Z. Yang, R. Al-Bahrani, A. C. Reid, S. Papanikolaou, S. R. Kalidindi, W. keng Liao, A. Choudhary, and A. Agrawal, Deep learning based domain knowledge integration for small datasets: Illustrative applications in materials informatics, in *2019 International Joint Conference on Neural Networks (IJCNN)* (2019).

[12] R. Cang, Y. Xu, S. Chen, Y. Liu, Y. Jiao, and M. Yi Ren, Microstructure representation and reconstruction of heterogeneous materials via deep belief network for computational material design, J. Mech. Des. **139** (2017).

[13] X. Li, Z. Yang, L. C. Brinson, A. Choudhary, A. Agrawal, and W. Chen, A deep adversarial learning methodology for designing microstructural material systems, in *ASME 2018 international design engineering technical conferences and computers and information in engineering conference* (2018).

[14] B. Sanchez-Lengeling and A. Aspuru-Guzik, Inverse molecular design using machine learning: Generative models for matter engineering, Science **361**, 360 (2018).

[15] D. Fokina, E. Muravleva, G. Ovchinnikov, and I. Oseledets, Microstructure synthesis using style-based generative adversarial networks, Phys. Rev. E **101**, 043308 (2020).

[16] L. Mosser, O. Dubrule, and M. J. Blunt, Reconstruction of three-dimensional porous media using generative adversarial neural networks, Phys. Rev. E **96**, 043309 (2017).

[17] L. Banko, Y. Lysogorskiy, D. Grochla, D. Naujoks, R. Drautz, and A. Ludwig, Predicting structure zone diagrams for thin film synthesis by generative machine learning, Commun. Mater. **1**, 1 (2020).

[18] R. Gómez-Bombarelli, J. N. Wei, D. Duvenaud, J. M. Hernández-Lobato, B. Sánchez-Lengeling, D. Sheberla, J. Aguilera-Iparraguirre, T. D. Hirzel, R. P. Adams, and A. Aspuru-Guzik, Automatic chemical design using a data-driven continuous representation of molecules, ACS Cent. Sci. **4**, 268 (2018).

[19] A. Gayon-Lombardo, L. Mosser, N. P. Brandon, and S. J. Cooper, Pores for thought: generative adversarial networks for stochastic reconstruction of 3d multi-phase electrode microstructures with periodic boundaries, Npj Comput. Mater. **6**, 1 (2020).

[20] D. P. Kingma and M. Welling, Auto-encoding variational bayes, in *Proceedings of the 2nd International Conference on Learning Representations* (2014).

[21] I. Goodfellow, J. Pouget-Abadie, M. Mirza, B. Xu, D. Warde-Farley, S. Ozair, A. Courville, and Y. Bengio, Generative adversarial nets, in *Advances in Neural Information Processing Systems*, Vol. 27 (2014).

[22] T. Guo, D. J. Lohan, R. Cang, M. Y. Ren, and J. T. Allison, An indirect design representation for topology optimization using variational autoencoder and style transfer, in *2018 AIAA/ASCE/AHS/ASC Structures, Structural Dynamics, and Materials Conference* (2018).

[23] X. Li, Y. Zhang, H. Zhao, C. Burkhart, L. C. Brinson, and W. Chen, A transfer learning approach for microstructure reconstruction and structure-property predictions, Sci. Rep. **8**, 1 (2018).

[24] R. Cang, H. Li, H. Yao, Y. Jiao, and Y. Ren, Improving direct physical properties prediction of heterogeneous materials from imaging data via convolutional neural network and a morphology-aware generative model, Comput. Mater. Sci. **150**, 212 (2018).

[25] S. Chun, S. Roy, Y. T. Nguyen, J. B. Choi, H. Udaykumar, and S. S. Baek, Deep learning for synthetic microstructure generation in a materials-by-design framework for heterogeneous energetic materials, Sci. Rep. **10**, 1 (2020).

[26] Z. Yang, X. Li, L. Catherine Brinson, A. N. Choudhary, W. Chen, and A. Agrawal, Microstructural materials design via deep adversarial learning methodology, J. Mech. Des. **140** (2018).

[27] A. Van Oord, O. Vinyals, and K. Kavukcuoglu, Neural discrete representation learning, in *Proceedings of the 31st International Conference on Neural Information Processing Systems* (2017).

[28] A. Van Oord, N. Kalchbrenner, and K. Kavukcuoglu, Pixel recurrent neural networks, in *Proceedings of The 33rd International Conference on Machine Learning* (2016).

[29] A. Van Oord, N. Kalchbrenner, O. Vinyals, L. Espeholt, A. Graves, and K. Kavukcuoglu, Conditional image generation with pixelcnn decoders, in *Proceedings of the 30th International Conference on Neural Information Processing Systems* (2016).

[30] N. Otsu, A threshold selection method from gray-level histograms, IEEE Trans. Syst. Man Cybern. Syst. **9**, 62 (1979).

[31] C. Peng-Heng and A. Preban, The effect of ferrite grain size and martensite volume fraction on the tensile properties of dual phase steel, Acta metall. **33**, 897 (1985).
[32] I. Jolliffe, *Principal Component Analysis* (Springer Verlag, New York, 1986).
[33] M. R. Akbarpour and A. Ekrami, Effect of ferrite volume fraction on work hardening behavior of high bainite dual phase (dp) steels, Mater. Sci. Eng. A **477**, 306 (2008).
[34] R. Armstrong, The influence of polycrystal grain size on several mechanical properties of materials, Metall. Mater. Trans. B **1**, 1169 (1970).